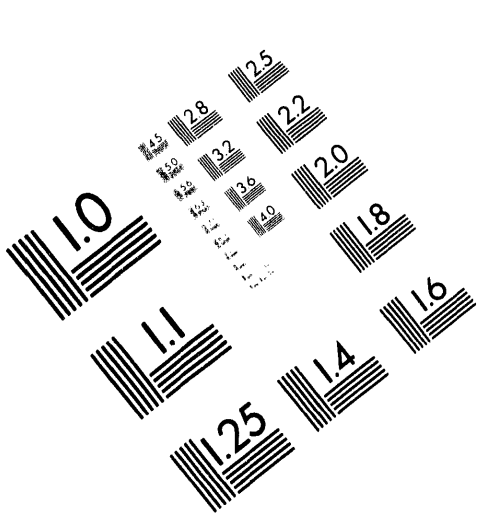

Association for Information and Image Management
1100 Wayne Avenue, Suite 1100
Silver Spring, Maryland 20910
301/587-8202

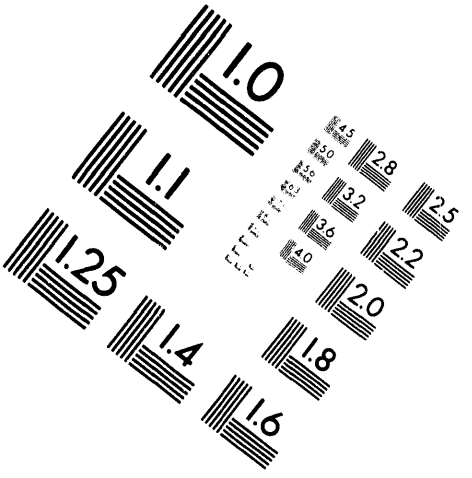

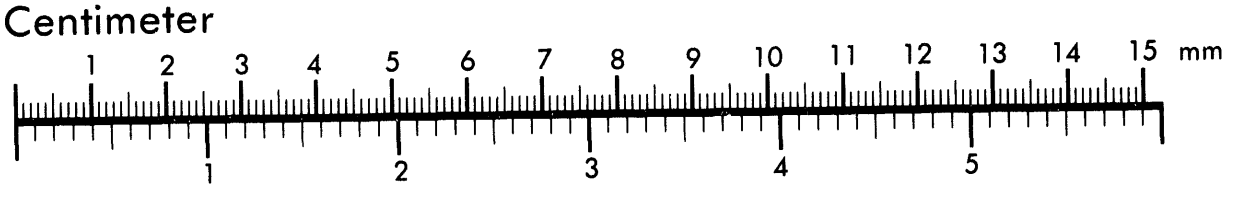

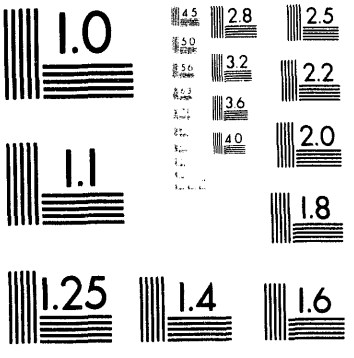

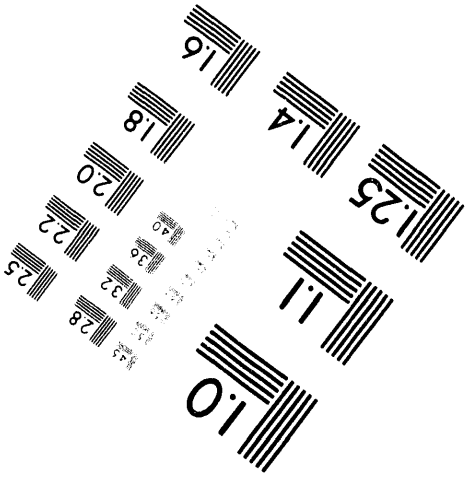

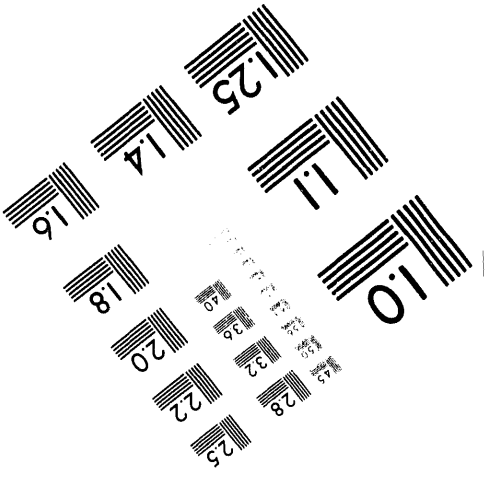

MANUFACTURED TO AIIM STANDARDS
BY APPLIED IMAGE, INC.

1 of 1

Numerical Studies on the Electromagnetic Properties of the Nonlinear Lorentz Computational Model for the Dielectric Media

Hirotada Abe[†] and Hideo Okuda

Princeton Plasma Physics Laboratory, Princeton University,

P.O. Box 451

Princeton, N.J. 08543

ABSTRACT

We study linear and nonlinear properties of a new computer simulation model developed to study the propagation of electromagnetic waves in a dielectric medium in the linear and nonlinear regimes. The model is constructed by combining a microscopic model used in the semi-classical approximation for the dielectric media and the particle model developed for the plasma simulations. It is shown that the model may be useful for studying linear and nonlinear wave propagation in the dielectric media.

[†]Permanent address: Department of Electronics and Informatics, Ryukoku University, 1-5 Yokotani, Oe-cho Seta, Otsu-shi 520-21, Japan.

DISTRIBUTION OF THIS DOCUMENT IS UNLIMITED

I. INTRODUCTION

A new computer simulation model,[1] called the nonlinear Lorentz Computational model, has recently been proposed to study electromagnetic wave propagation in linear and nonlinear dispersive solid-state media.

The original Lorentz model of the atom, which treats the atom as a harmonic oscillator, provides a very good description of the linear electromagnetic properties of the dielectric media.[2]

In order to model the response of a nonlinear dielectric medium, a semi-classical model[3,4,5] is used to represent the electrical behavior of the nonlinear dispersive solid-state media. To include a nonlinearity arising from the intrinsic quantum effects, this model is constructed by extending the Lorentz model for the dielectric media[2] so that the electrons in the atom are allowed to include a nonlinear restoring force.

It is well known that, according to the quantum-mechanical theory of the nonlinear susceptibility, each atom possesses many energy eigen values and has more than one resonance frequency. Since the present model allows only one resonance frequency for each atom, it provides a good model for only the cases in which all wave frequencies of interest are off-resonant or well seperated from the resonance frequency. Nonetheless, many useful applications are expected to exist even in these limited cases.

The details of the model differ depending upon whether or not the

medium possesses an inversion symmetry. The tensor properties of the susceptibility cannot be specified unless the internal symmetries of the medium are completely known. One of the most important cases is that of a material which is isotropic and centrosymmetric.[5] Examples of such materials are liquids, gases, amorphous solids such as glass, and even many crystals displaying inversion symmetry. In this paper, we focus our attention on these cases and find that such medium induces a cubic nonlinear contribution to the polarization which causes the third order susceptibility in terms of the electric field.

To numerically solve both Maxwell's equations for the fields and the equation of motion for many charged particles or dipoles self-consistently, the model is constructed by adopting the numerical techniques which have been developed in the electromagnetic particle simulation of plasmas.[6,7] Here only the equation of motion for charged particle is modified from that in the original particle simulation model for free electrons and ions in order to represent the linear and the nonlinear properties of the dispersive solid-state media.

Another approach to simulate wave propagation in linear and nonlinear dielectric materials is to use the finite-difference method in the time domain in which Maxwell's equations are solved directly together with linear and nonlinear susceptibilities given as frequency-dependent functions a priori.[8,9,10]

Our nonlinear Lorentz Computational model differs physically and numerically from this model. We may apply our model to study the femtosecond phenomena such as soliton propagation[11] or opitical switching in a glass.[12,13,14] As the nanosecond phenomena, a high-power soliton generation in a ceramic[15] may be simulated using our model. These should be studied extensively because of its importance in their applications to optical microelectronics, communication engineering, and electrical engineering.

II. THEORETICAL REVIEW AND SIMULATION MODEL

A. Nonlinear Lorentz Computational Model

Let us describe in detail the mathematical method to model the nonlinear Lorentz computational model here. Microscopically, the simplest dielectric material can be considered as an isotropic and locally uniform collection of a large number of electric dipoles with the eigen frequency ω_0 for the oscillating electric field. We, therefore, assume in our model that a large number of electric dipoles are uniformly distributed in the system, where the ions are assumed fixed spatially and the electrons oscillate around the ions.

The motion of the electrons in the presence of an electric field $\mathbf{E}$ and a magnetic field $\mathbf{B}$ is given by[5]

$$\frac{d\mathbf{x}_j}{dt} = \mathbf{v}_j \ ,$$

$$\frac{d\mathbf{v}_j}{dt} = -\frac{e}{m}\left(\mathbf{E}+\mathbf{v}_j\times\mathbf{B}\right) - {\omega_0}^2 f_j(\mathbf{x}_j-\mathbf{x}_{0j}) - \Gamma_0\mathbf{v}_j\ ,$$
$$f_j = 1 + \delta_3\frac{{\omega_0}^2}{{c_m}^2}(\mathbf{x}_j-\mathbf{x}_{0j})\cdot(\mathbf{x}_j-\mathbf{x}_{0j})\ , \qquad (1)$$

where $\mathbf{x}_j$ and $\mathbf{v}_j$ are the position and the velocity of the j-th electron, $\mathbf{x}_{j0}$ is its equilibrium position, Γ_0 is a small friction coefficient, δ_3 is a numerical constant for the cubic nonlinearity for the dielectric media, and c_m is the velocity used for normalization and its definition will appear after Eq. (3). In the present one-dimensional limit, Eq. (1) agrees with earlier results.[1]

In the case of $\delta_3 < 0$, Eq. (1) is unstable for a large wave amplitude. In order to stabilize the equation of motion, f_j is approximated by

$$f_j = \delta_{3r} + (1-\delta_{3r})\exp\left[\frac{\delta_3}{(1-\delta_{3r})}\frac{{\omega_0}^2}{{c_m}^2}(\mathbf{x}_j-\mathbf{x}_{0j})\cdot(\mathbf{x}_j-\mathbf{x}_{0j})\right]\ , \qquad (2)$$

for a negative δ_3 where δ_{3r} is a non-negative numerical constant less than unity. For a small displacement, Eq. (2) is reduced to Eq. (1).

Equation (1) is finite-differenced by the leapfrog scheme and solved self-consistently together with Maxwell's equations[6,7] for the electric and magneteic fields. Writing $\mathbf{E} = \mathbf{E}^T + \mathbf{E}^L$ and $\mathbf{B} = \mathbf{B}^T$, Maxwell's equations are given by

$$\nabla\times\mathbf{E}^T = -\frac{\partial\mathbf{B}^T}{\partial t},$$

$$\nabla \times \mathbf{B}^T = \frac{1}{{c_m}^2}\frac{\partial \mathbf{E}^T}{\partial t} + \mu_0 \mathbf{J}^T,$$
$$\nabla \cdot \mathbf{E}^L = \frac{\rho}{\varepsilon_0},$$
$$\nabla \cdot \mathbf{B}^T = 0. \tag{3}$$

Here c_m is the speed of light in a dielectric in the case of the infinitely-high frequency,

$$c_m = \frac{c}{\sqrt{\varepsilon_m}},$$

where c is the speed of light in vacuum and ε_m is the dielectric constant relative to vacuum representing the effects of contribution from the dipoles with eign frequencies much higher than those in the system. The upperscripts T and L indicate the transverse and longitudinal components of a vector $\mathbf{Q}$ satisfying

$$\nabla \cdot \mathbf{Q}^T = 0,$$
$$\nabla \times \mathbf{Q}^L = 0.$$

The current and charge densities $\mathbf{J}$ and ρ are given by

$$\mathbf{J} = \sum_{j=1}^{N} -e\, \mathbf{v}_j \delta(\mathbf{x} - \mathbf{x}_j) + \mathbf{J}_{ext},$$
$$\rho = \sum_{j=1}^{N} e\, \left[-\delta(\mathbf{x} - \mathbf{x}_j) + \delta(\mathbf{x} - \mathbf{x}_{j0})\right], \tag{4}$$

where N is the total number of the dipoles in the system and $\mathbf{J}_{ext}$ is an external current to inject an electromagnetic wave into the system.

B. Fresnel's formula for the case of the normal incidence

We assume that the boundary between vacuum and a dielectric medium is planar and located at $x = x_B$. Let a linearly polarized monochromatic plane wave with frequency ω coming from the left-side space $x < x_B$ impinge upon this boundary. In the case of the one-dimensional simulation studied here, we can treat only the normal incidence. For the solution of this boundary-value problem, we need to consider three waves, an incident wave, a refracted wave, and a reflected wave, whose complex electric amplitude are denoted by A, B, and C, respectively. We get the resulting superposition of the incident and reflected waves in vacuum denoted by a subscript v and the refracted wave in the dielectric medium denoted by a subscript d as

$$E_{zv} = \{A \exp[+ik_v(x - x_B)] + C \exp[-ik_v(x - x_B)]\} \exp(-i\omega t),$$
$$E_{zd} = B \exp[+ik_d(x - x_B)] \exp(-i\omega t), \tag{5}$$

where their wave numbers k_v and k_d are related to the refractive index n by

$$\frac{k_d}{k_v} = n. \tag{6}$$

The boundary conditions for E_z and $B_y = 1/\omega \partial E_z/\partial x$ derived from Eq. (3) require

$$A + C = B,$$

and

$$A - C = -\frac{k_d}{k_v} B = -nB. \tag{7}$$

The ratios of the reflected and the refracted wave amplitudes to the incident wave amplitude are given by

$$\begin{aligned} \frac{C}{A} &= \frac{1-n}{1+n}, \\ \frac{B}{A} &= \frac{2}{1+n}. \end{aligned} \tag{8}$$

C. Dispersion relation in the nonlinear dielectric medium

In the non-conducting material, imagine that the electric field $\mathbf{E}$ is imposed on the electron charge $-e$. This charge is displaced from the ionic charge $+e$ in the direction opposite to the electric field $\mathbf{E}$. We can assume the ionic charge $+e$ which carries the ionic mass M to be stationary. Thus an electric dipole moment $(+e, -e)$ is directed parallel to E and so the polarization vector $\mathbf{P}$ is given by

$$\mathbf{P} = -n_d \, e \, \mathbf{s} \, , \tag{9}$$

where $\mathbf{s}$ is the moment arm vector and n_d is the number of the electrons per unit volume. The electric displacement $\mathbf{D}$ is given by

$$\mathbf{D} = \varepsilon_m \varepsilon_0 \mathbf{E} + \mathbf{P}. \tag{10}$$

In this case, the current in Maxwell's equation, Eq. (3), is restricted to only the poralization current as

$$\mathbf{J} = \dot{\mathbf{P}}. \tag{11}$$

For the transverse electric field $\mathbf{E}^T$ which satisfies $\nabla \cdot \mathbf{E}^T = 0$, we get

$$\nabla^2 \mathbf{E}^T - \frac{1}{c_m^2} \ddot{\mathbf{E}}^T = \mu_0 \ddot{\mathbf{P}}^T. \tag{12}$$

Assuming a linearly polarized wave with the frequency ω,

$$E_z{}^T = \tilde{E}(x) \exp(-i\omega t), \qquad E_x{}^T = E_y{}^T = 0, \tag{13}$$

we find the following Duffing's second order ordinary differential equation,[16]

$$\ddot{z} + \omega_0{}^2 z + a_3 z^3 = \frac{e}{m} \tilde{E}(x) \exp(i\omega t), \tag{14}$$

where $a_3 = \delta_3 \omega_0{}^4 / c_m{}^2$. When the wave amplitude $\tilde{E}$ is small but finite, an approximate solution[3] is given by

$$z(t) = z_1 \exp(i\omega t) + z_3 \exp(i3\omega t), \tag{15}$$

where

$$\begin{aligned} z_1 &= \frac{e}{m} \frac{\tilde{E}(x)}{\omega_0{}^2 - \omega^2} \left[1 - \frac{3}{4} \frac{e^2}{m^2} \frac{a_3 \tilde{E}^2(x)}{(\omega_0{}^2 - \omega^2)^3} \right], \\ z_3 &= -\frac{z_1}{4} \frac{e^2}{m^2} \frac{a_3 \tilde{E}^2(x)}{(9\omega^2 - \omega_0{}^2)(\omega_0{}^2 - \omega^2)^3}. \end{aligned} \tag{16}$$

Let us assume that the friction coefficient Γ_0 is sufficiently small. Substituting $s = z$ and $\mathbf{E}^T = \tilde{E}(x)\hat{z}$ to Eq. (14) in the presence of a cubic nonlinearity ($\delta_3 \neq 0$) for the transverse electromagnetic wave $\tilde{E}_z$, we get the following nonlinear differential equation,

$$\frac{d^2}{dx^2}\tilde{E}_z + \frac{\omega^2}{c_m^2}\tilde{E}_z = \\ -\frac{\omega^2}{{c_m}^2}\frac{{\omega_p}^2}{{\omega_0}^2 - \omega^2 - i\omega\Gamma_0}\left[1 - \frac{3}{4}\,\delta_3\left(\frac{e\,{\omega_0}^2}{m\,c_m}\right)^2 \frac{\tilde{E}^2(x)}{({\omega_0}^2 - \omega^2)^3}\right]\tilde{E}_z, \qquad (17)$$

where ω_p is the plasma frequency defined by $\omega_p = (n_d e^2/\epsilon_0 m)^{1/2}$.

Assuming a plane wave $\tilde{E}(x) = E\exp(+ikx)$, we get[1]

$$\left(\frac{c\,k}{\omega}\right)^2 = \varepsilon_m + \frac{{\omega_p}^2}{{\omega_0}^2 - \omega^2 - i\omega\Gamma_0}\left[1 - \frac{3}{4}\,\delta_3\left(\frac{e\,{\omega_0}^2}{m\,c_m}\right)^2 \frac{\tilde{E}^2(x)}{({\omega_0}^2 - \omega^2)^3}\right]. \qquad (18)$$

Averaging this spatially, we obtain the nonlinear dielectric constant relative to vacuum, $\varepsilon(\omega)$:

$$\varepsilon(\omega) = n^2 \equiv \left(\frac{c\,k}{\omega}\right)^2 = \varepsilon_m + \chi^{(1)}(\omega) + \chi^{(3)}(\omega)\,E^2, \qquad (19)$$

where the linear and nonlinear susceptibilities $\chi^{(1)}(\omega)$ and $\chi^{(3)}(\omega)$ are given by

$$\chi^{(1)}(\omega) = \frac{{\omega_p}^2}{{\omega_0}^2 - \omega^2 - i\omega\Gamma_0}, \\ \chi^{(3)}(\omega) \sim -\frac{3}{8}\,\delta_3\left(\frac{e\,{\omega_0}^2}{m\,c_m}\right)^2 \frac{{\omega_p}^2}{({\omega_0}^2 - \omega^2)^4}. \qquad (20)$$

The nonlinear refractive index can be approximated by

$$n(\omega, E^2) = n_0(\omega) + n_2 \, E^2, \tag{21}$$

where

$$\begin{aligned} n_0 &= \left[\varepsilon_m + \chi^{(1)}(\omega) \right]^{1/2} , \\ n_2 &= \frac{\chi^{(3)}}{2n_0} . \end{aligned} \tag{22}$$

The second term of the righthand side of Eq. (21) represents the high-frequency Kerr effect so that the balance between the nonlinearity and the linear dispersive properties in this wave dispersion equation may account for propagation of the envelope soliton.[11]

The change of wavelength, $\Delta\lambda$, scales with the wave amplitude E as

$$\Delta\lambda = \lambda_m n_2 E^2, \tag{23}$$

where $\lambda_m = 2\pi c_m/\omega$.

III. SIMULATION RESULTS

Two examples have been considered for the steady state wave propagation using the model: the first one concerns with the phenomenon in a linear dielectric material placed in vacuum and the second for a uniform dielectric medium with cubic nonlinearity. While Eq. (1) is valid in three

dimensions, for simplicity only a one-dimensional model was considered, in which all the electromagnetic fields vary with x only.

In the simulations discussed in the following, we have introduced a characteristic frequency ω_N and a grid length Δ, which are used for the normalization of the simulation parameters, and they are used to scale the simulation results to those in various cases.

For simplicity, let us assume $\varepsilon_m = 1.0$. As typical examples, we assume $\omega_N = 10^{14}\ rad/s$ in the optical engineering applications and $\omega_N = 10^{10}\ rad/s$ in the electrical engineering applications. The vacuum wavelengths for the pumping frequency $\omega = 2.0\ \omega_N$ used in this work become $\lambda_v = 9.425\ \mu m$ and $\lambda_v = 94.25\ mm$. The speed of light $c = 3 \times 10^8 m/s$ corresponds to $20.0\ \omega_N \Delta$ in the simulation and so its wavelength λ_v is $62.83\ \Delta$, which means $\Delta = 0.15\ \mu m$ and $\Delta = 1.5\ mm$, respectively. By using different characteristic frequency ω_N and ε_m, a different dielectric material can be studied.

The length of the one-dimensional system, L, is taken 2048 spatial grids, $L = 2048\Delta$. The absorbing boundary condition[17] is imposed on the electromagnetic waves so that they are damped away in the ramp regions at the left and right edges ($0 \leq x \leq L/8$ and $7L/8 \leq x \leq L$) by means of ramp functions. The eigen frequency ω_0 and the plasma frequency ω_p were chosen to be $4.0\ \omega_N$ and $4.62\ \omega_N$ and the friction Γ_0 was chosen to be $2.0 \times 10^{-5}\ \omega_N$ for the examples given here. This means

$\varepsilon(0) = 2.33$ and the refractive index n calculated from Eq. (19) is 1.667 for the wave frequency $\omega = 2.0\,\omega_N$. The linear complex relative dielectric constant ε vs ω for this dielectric medium is shown in Fig. 1.

The total number of the dipoles in the system is 25,600. The normalized time step $\omega_N \Delta t$ is chosen to be 0.04.

As a method of the spatial interpolation for charge and current sharing and the field-quantity interpolation, the linear spline has been used. To calculate the field quantity,[6,7] we use the fast Fourier transformation (FFT) method with the k-space smoothing using the Gaussian filter with its radius $R = \Delta$.

A. Reflection and refraction at the boundary

We first demonstrate the accuracy of the model by simulating the wave refraction and reflection at the planar interface between vacuum and the dielectric medium. Shown in Fig. 2(a) is the instantaneous plot of E_z vs x for the steady state wave propagation, where an electromagnetic wave with its frequency of $\omega = 2.0\,\omega_N$ is excited in vacuum at $x = L/8$ by an oscillating current $J_z = J_0 e^{-i\omega t}$, where J_0 is the current amplitude and is held constant in time. The linear dielectric media is located between $x = L/2$ and $x = 15L/16$ ($\delta_3 = 0$).

Figures 2(b) and (c) are the interferograms $E_{zs}(x)$ and $E_{zc}(x)$ between

E_z and the wave source signals $\sin(\omega t)$ and $\cos(\omega t)$ calculated by[18]

$$E_{zs}(t,x) = \frac{2}{MT}\int_{t-MT}^{t} E_z(t',x)\sin(\omega t')dt',$$
$$E_{zc}(t,x) = \frac{2}{MT}\int_{t-MT}^{t} E_z(t',x)\cos(\omega t')dt', \qquad (24)$$

where $T = 2\pi/\omega$ and M is a positive intger ($M = 20$). Substituting the first and second equations of Eq. (5) into the first equation of Eq. (24), we get $E_{zs}(t,x) = (A+C)\cos(k_v x + \phi_{vs})$ and $E_{zs}(t,x) = B\cos(k_d x + \phi_{ds})$, respectively. From Fig. 2(b), we can see that the first condition of the boundary conditon Eq. (7) exactly holds. Substitution of the first and second equations of Eq. (5) into the second equation of Eq. (24) yields $E_{zc}(t,x) = (A-C)\cos(k_v x + \phi_{vc})$ and $E_{zc}(t,x) = B\cos(k_d x + \phi_{dc})$. Measuring A, B, and C from Figs. 2(b) and (c) and substituing these values into Eq. (8), we get the value of the refractive index, $n_d = 1.66$.

In the dielectric region, the wavelength becomes shorter compared with that in the vacuum region. The wavelengths in vacuum and in the dielectric in the uniform space are calculated to be $\lambda_v = 62.83\Delta$ and $\lambda_d = 37.69\Delta$, respectively.

We have calculated the interferograms between the electric field E_z and the pump wave signal $J_z = J_0 e^{-i\omega t}$ in the complex function. Figure 2(d) is the wave number spectrum calculated over the space between $x = L/8$ and $x = 7L/8$, where a negative wave number in the figure corresponds to a negative phase velocity. Here, we can measure the wave numbers and

convert it to the wavelength quite accurately. The digital measurement of the wavelength may cause to produce error of the order of or less than 1 part in 1,000. The electromagnetic wave is refracted and reflected at the left edge of the dielectric. There is no reflection at the right edge, because it is embedded in the wave absorbing region or the ramp region.[17] The right, middle, and left peaks correspond to the refracted, incident, and reflected waves, respectively. The wavelengths in vacuum and in the dielectric are measured to be $\lambda_v = 62.52\Delta$ and $\lambda_d = 38.13\Delta$, respectively. Major part of the small discrepancy between the theoretically calculated values and the measured values may be attributed to the effects of the finite-sized gird[19] and of the finite size of the simulation system, because the theory assume the gridless and the infinite space.

When we changed the position of the right boundary slightly or place the dielectric medium between $x = L/2$ and $x = 7L/8$ which was also a left edge of the right absorption region, we found a slightly different result: The fourth small peak is accompanied on the left side of the third peak as a result of reflection of the right boundary of the dielectric medium. The wavelengths in vacuum and in the dielectric are measured to be $\lambda_v = 63.09\Delta$ and $\lambda_d = 38.18\Delta$, respectively.

The energies associated with the incident, reflected, and refracted waves may be proportional to their peak amplitude times its base width in Fig. 2(c). Their measured ratio are 1.0 : 0.05 : 0.74, which can be

compared with $A^2 : C^2 : B^2 = 1.0 : 0.06 : 0.56$ calculated from Eq. (8).

B. Measurement of the cubic order nonlinearities

In this case the dielectric medium is assumed to be placed between $x = L/16$ and $x = 15L/16$ and to have cubic nonlinearities of $\delta_3 = +2.2 \times 10^6$ or $\delta_3 = -2.2 \times 10^6$. For negative δ_3 we assume $\delta_{3r} = 0$ in Eq. (2). An electromagnetic wave with its frequency of $\omega = 2.0\ \omega_N$ is excited at $x = L/8$ in the dielectric medium by an oscillating current $J_z = J_0 e^{-i\omega t}$. This system can be considered to be a uniform nonlinear dielectric medium except for in the ramp regions ($0 \leq x \leq L/8$ and $7L/8 \leq x \leq L$) located at the egdes of the system. In other words, we create the numerical illusion of an infinite space by this artificial boundary damping the electromagnetic wave numerically.

To confirm the relation Eq. (23), we have carried out many runs, changing the magnitude of the wave source current and its sign of δ_3. Among these runs, two typical runs are shown here: one is a run with the weak wave excitation in the dielectric with $\delta_3 = +2.2 \times 10^6$ and the other is a run with the strong wave excitation in the dielectric with $\delta_3 = -2.2 \times 10^6$.

Figure (3) shows the instantaneous magnitudes of E_z vs x for the weak and strong wave excitaions. In the case of the weak wave excitation, almost coherent wave is seen to be excited, while in the case of the strong wave excitation some noises are seen to be mixed with the coherent wave.

Figure (4) shows their interferograms $E_{zs}(t,x)$ for both runs. Some nonlinear coherent modes with longer wavelengths appear in the strong excitation and so the wave amplitude is modulated spatially. The phenomenon of this self-phase modulation may be practically important, because it may be applied to a kind of the nonlinear optical switching.[14] Time-averaging eliminates its noise from the instantaneous wave form and thus clearer sinusoidal wave form is seen in Fig. 4(a) than that in Fig. 3(a).

Figure (5) shows their corresponding wave number spectra. In the weak excitation, only a single peaked mode is seen and so its wave number can be measured quite accurately. In the strong excitation, on the other hand, the spectrum is split into three peaks and therefore the measurement of the wave number becomes impossible.

Figure (6) shows the frequency spectra at $x \sim L/4$. In the strong wave excitation, a small peak with frequency of $\omega \sim 1.7\omega_0$ appears due to the nonlinearity. This mode may be accountable for the noises seen in Fig. 3(b), which shows the instantaneous plot E_z vs x.

Figure (7) shows $\Delta\lambda$ vs $(\delta_3/|\delta_3|)\ {E_z}^2$. The solid straight line in this figure shows the relation of Eq. (23). The circles show the measured values in the 16 runs. The theoretical prediction, Eq. (23), agrees with the measured values quite well. From this figure, we can see that this measurement method holds quite good accuracy and that difference of

order of 1/10 grid length may be detected for wavelength deviation $\Delta\lambda$ or even better resolution may be obtained. From this measurement, we can see that the curve slightly concaves upwards. This inclination suggests existence of the higer order structure of nonlinearitis in the system.

IV. DISCUSSION AND CONCLUSION

While the model for the nonlinear media is assumed a simple form in the examples given here, it can be improved further depending on the goal of the simulations. This can be achieved by increasing the accuracy of the model to include the detailed microscopic structures of the dielectric media. For example, it is possible to increase the number of the species of the harmonic oscillators. Furthermore, we may be able to include lattice oscillations of nuclei arising from the quantum mechanical effects by including the motion of the ions which are assumed frozen in this work. In this way, Raman scattering may be included within the classical approximation. Since our model follows the individual motion of the electrons, the model can be used to study, for example, light amplification caused by the population inversion. While we considered wave propagation in a dielectric medium, models for electromagnetic wave propagation in a metal or in a semi-conductor can be constructed by adopting the Drude model[20] or the free carrier model for the conducting current.

In the case of the strong nonlinearity, the Duffing equation[16] which governs the equation of motion of the dipole is well known to show quite interesting phenomena such as hysteresis or chaos. We expect that these nonlinear optical phenomena may be studied by our model. These suggestions should be further investigated extensively, by comparing the simulation results with the experimental and theoretical results. This in turn clarifies the modeling capability or the way to improve the model.

In conclusion, we have studied the physical and computational properties of the nonlinear Lorentz computational model for the dielectric medium. Although this study has remained within the framework of the relatively weak nonlinear system where the small wave amplitude expansion is permitted, both linear and nonlinear wave propagations have been studied in detail and the results are found to be in good agreement with the theoretical predictions verifying the validity of the model.

Acknowledgment

We acknowledge Prof. Y. R. Shen for useful discussions and his valuable comments. We appreciate Dr. H. Ikezi for his comment on an application to the electrical engineering. We also thank Profs. R. W. Dutton and K. Iizuka for their interest and encouragement.

This work was supported by the U.S. Department of Energy Contract No. DE-AC02-76-CHO-3073.

REFERENCES

1. H. Abe and H. Okuda, Opt. Lett. 19, 10 (1994).
2. A. Sommerfeld, *Optics* (Academic Press, New York, 1954), Chap. 3, p. 89.
3. G. C. Baldwin, *An Introduction to Nonlinear Optics* (Plenum Press, New York, 1969), Appendix 5, p. 143.
4. Y. R. Shen, *The Principles of Nonlinear Optics* (John Wiley & Sons, New York, 1984).
5. R. W. Boyd, *Nonlinear Optics* (Academic Press, San Diego, 1992), Chap. 1, p. 29.
6. A. T. Lin, J. M. Dawson and H. Okuda, Phys. Fluids 17, 1995 (1975).
7. H. Abe and S. Nakajima, J. Phys. Soc. Jpn. 56, 3899 (1987).
8. P. M. Goorjian and A. Taflove, Opt. Lett. 17, 180 (1992).
9. P. M. Goorjian, A. Taflove, R. M. Joseph and S. C. Hagness, IEEE J. Quantum Electronics 28, 2416 (1992).
10. R. M. Joseph, P. M. Goorjian and A. Taflove, Opt. Lett. 18, 491 (1993).
11. A. Hasegawa and F. D. Tappert, Appl. Phys. Lett. 23, 142 (1973).
12. H. Kawaguchi, Opt. Lett. 10, 410 (1985).
13. H. G. Winful, Opt. Lett. 11, 33 (1986).

14. N. J. Doran and D. Wood, Opt. Lett. 13, 56 (1988).

15. H. Ikezi, J. S. DeGrassie and J. Drake, Appl. Phys. Lett. 58, 986 (1991).

16. P. Hagedorn, *Non-Linear Oscillations* (Clarendon Press, Oxford, England, 1988), Chap. 1, p. 35.

17. P. C. Liewer, A. T. Lin, J. M. Dawson and M. Z. Caponi, Phys. Fluids 24, 1364 (1981).

18. H. Abe, R. Itatani and H. Momota, Phys. Fluids 22, 1533 (1979).

19. H. Abe, N. Sakairi, R. Itatani and H. Okuda, J. comput. Phys. 63, 247 (1986).

20. K. D. Möller, *Optics* (University Science Books, Mill Valley CA, 1988), Chap. 7, p. 288.

FIGURE CAPTIONS

Fig. 1 The linear dielectric constant relative to vacuum, $\varepsilon(\omega) = 1+\chi^{(1)}(\omega)$, with the parameters of $\varepsilon(0) = 2.33$, $\varepsilon(\infty) = 1.0$, $\omega_0 = 4.0\,\omega_N$, and $\Gamma_0 = 2.0 \times 10^{-5}\,\omega_N$.

Fig. 2 Results of the refraction and reflection at the plane boundary. The magnitude of the electric field is normalized by $eE_z/(m{\omega_N}^2\Delta)$: (a) the instantaneous plot of $E_z(t,x)$ at $t = 320\,\omega_N$; (b) the interferogram plot of $E_{zs}(t,x)$ at $t = 314\,{\omega_N}^{-1}$; (c) the interferogram plot of $E_{zc}(t,x)$ at $t = 314\,{\omega_N}^{-1}$; (d) the wave number spectrum of E_z at $t = 314\,{\omega_N}^{-1}$. The abscissa m is related to the wave number $k = 2\pi m/L$ and the ordinates for ${E_z}^2$. The negative m corresponds to the negative phase velocity.

Fig. 3 Instantaneous plot of $E_z(t,x)$ at $t = 320\,\omega_N^{-1}$. The magnitude of the electric field is normalized by $eE_z/(m{\omega_N}^2\Delta)$: (a) for weak excitation; (b) for strong excitation.

Fig. 4 Interferogram plot of $E_{zs}(t,x)$ at $t = 314\,{\omega_N}^{-1}$. The magnitude of the electric field is normalized by $eE_z/(m{\omega_N}^2\Delta)$: (a) for weak excitation; (b) for strong excitation.

Fig. 5 Wave number spectrum of E_z at $t = 314\,{\omega_N}^{-1}$: (a) for weak excitation; (b) for strong excitation.

Fig. 6 Wave frequency spectrum of E_z at $x \sim L/4$: (a) for weak excitation; (b) for strong excitation.

Fig. 7 Comparison of $\Delta\lambda = \lambda_m n_2 E^2$ in Eq. (23) (straight line) with the measured values of $\Delta\lambda$ and ${E_z}^2$ (open circles). The abscissa and ordinate show $(\delta_3/|\delta_3|)\ {E_z}^2$ and $\Delta\lambda$ in unit of grid length Δ. The relation of Eq. (23) is shown by the solid straight line.

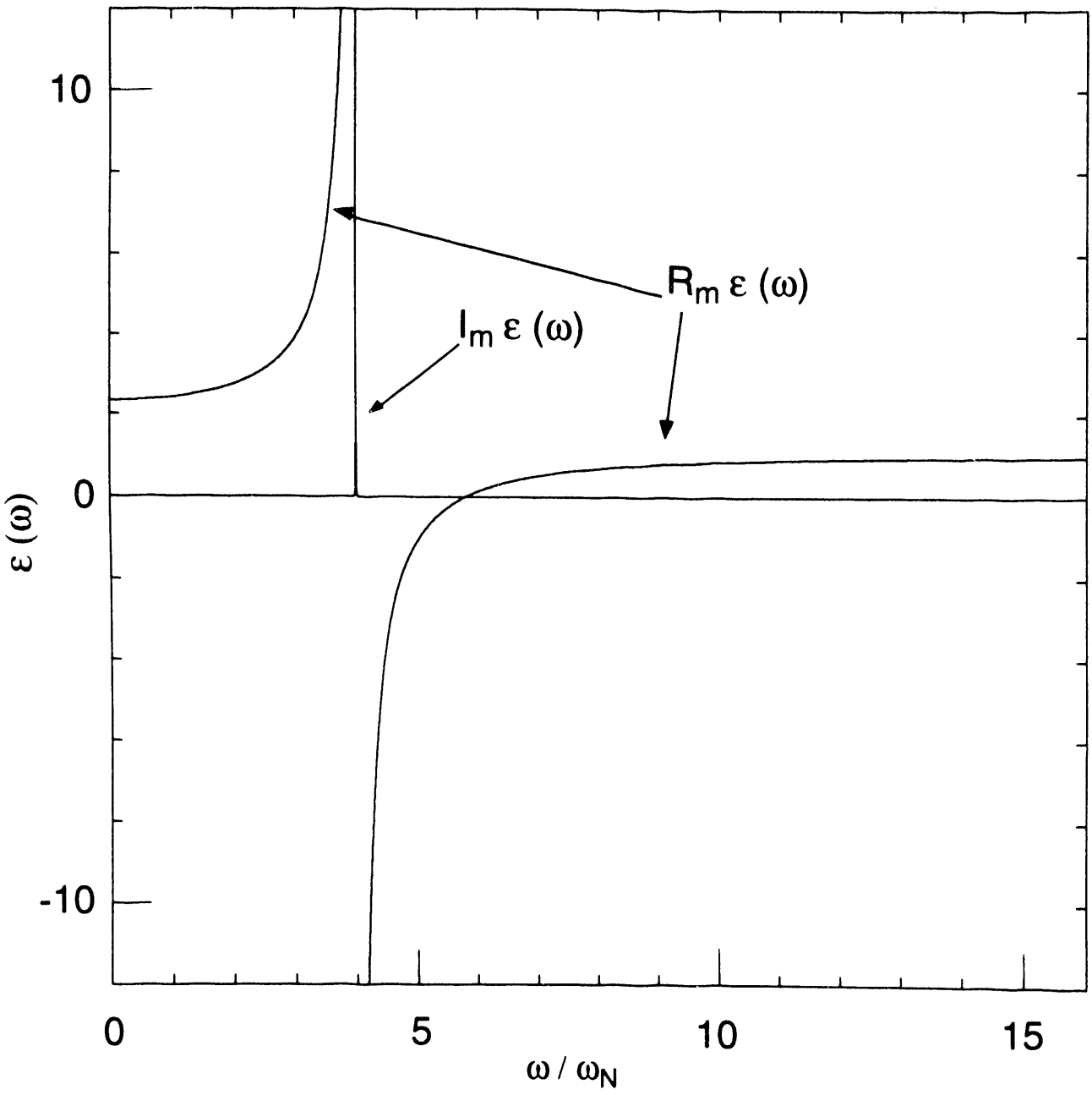

Fig. 1

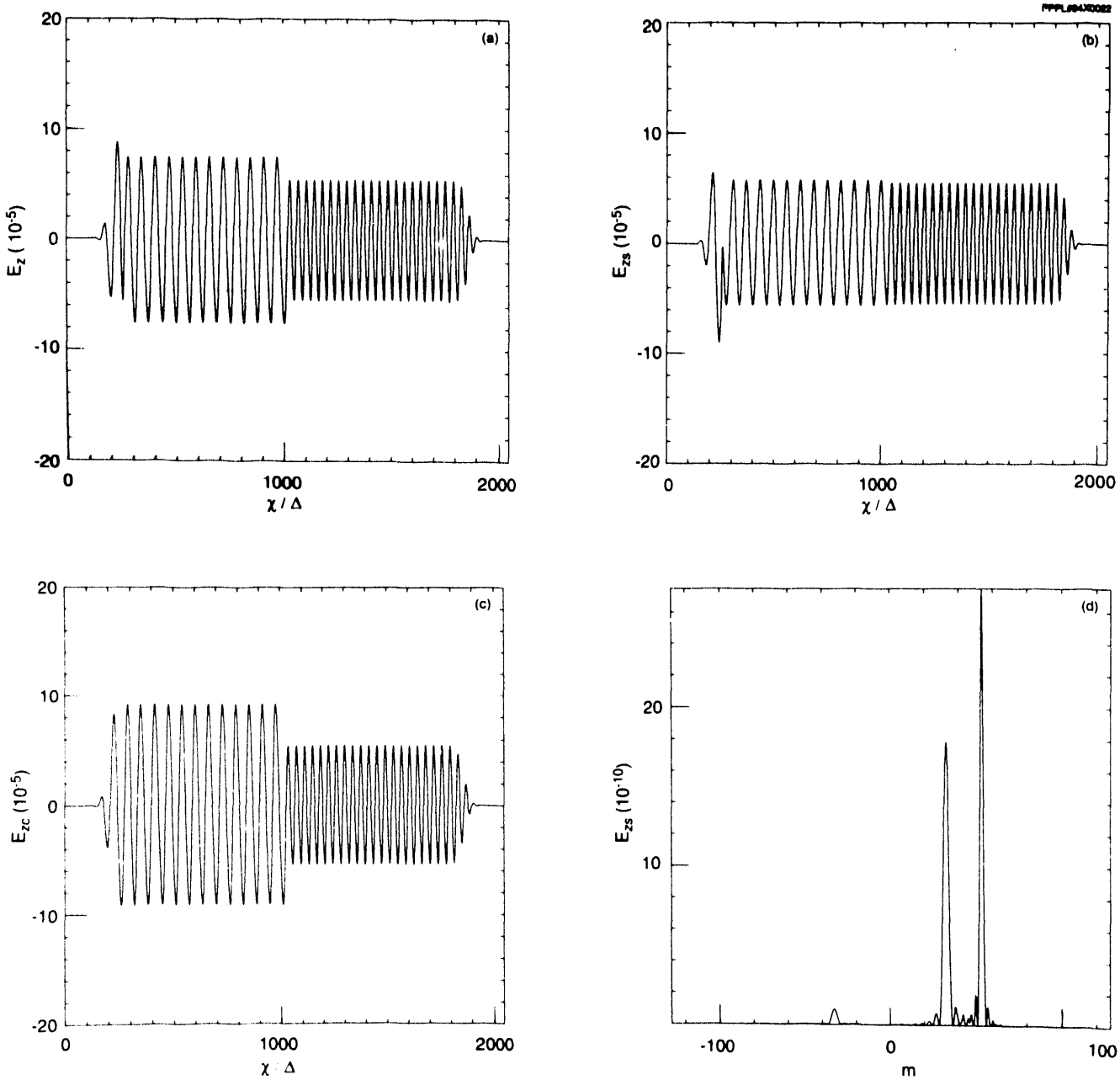
(a)
(b)
(c)
(d)
E_z (10^{-5})
E_{zs} (10^{-5})
E_{zc} (10^{-5})
E_{zs} (10^{-10})
χ / Δ
m
20
10
0
-10
-20
1000
2000
-100
100

Fig. 2

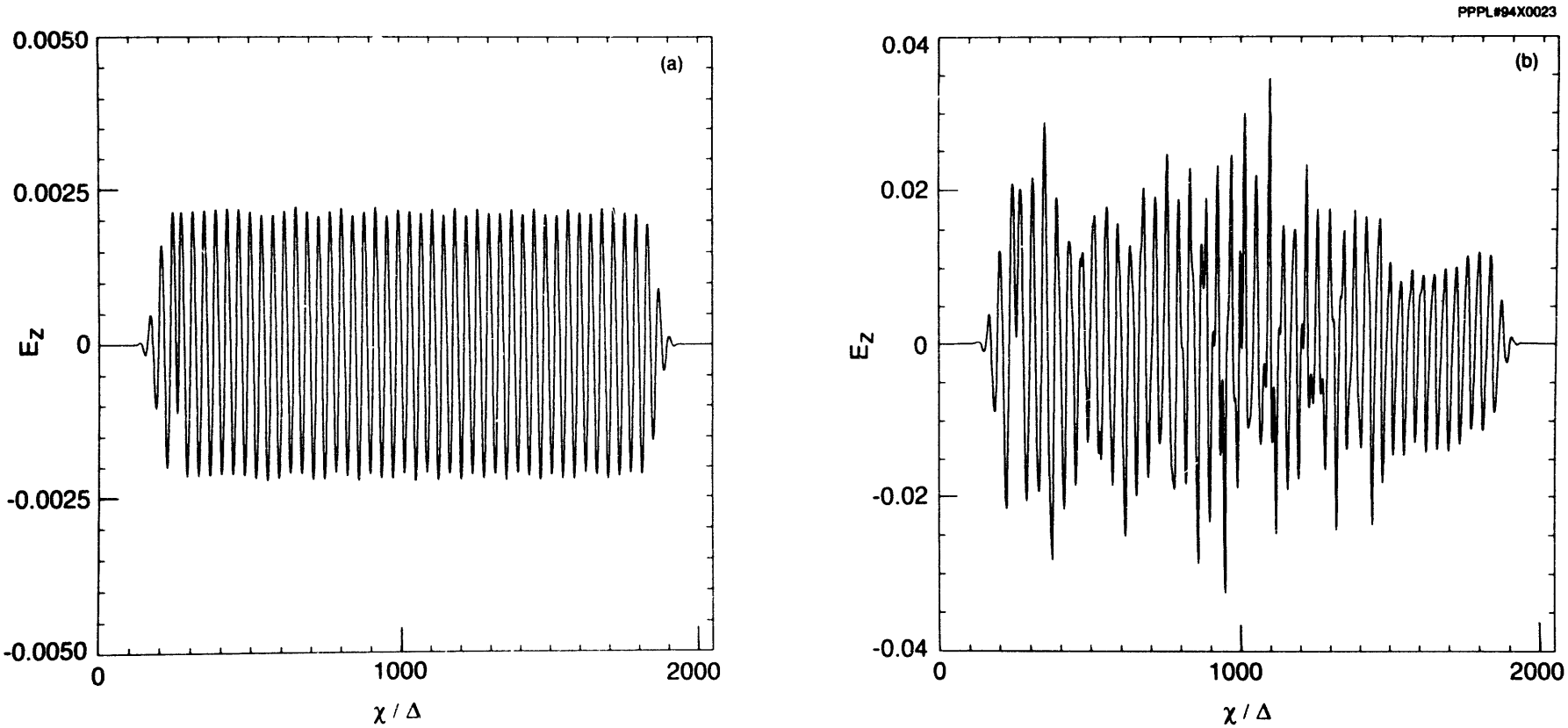
PPPL#94X0023
(a)
(b)
0.0050
0.0025
0
-0.0025
-0.0050
0.04
0.02
-0.02
-0.04
E_z
0
1000
2000
χ / Δ

Fig. 3

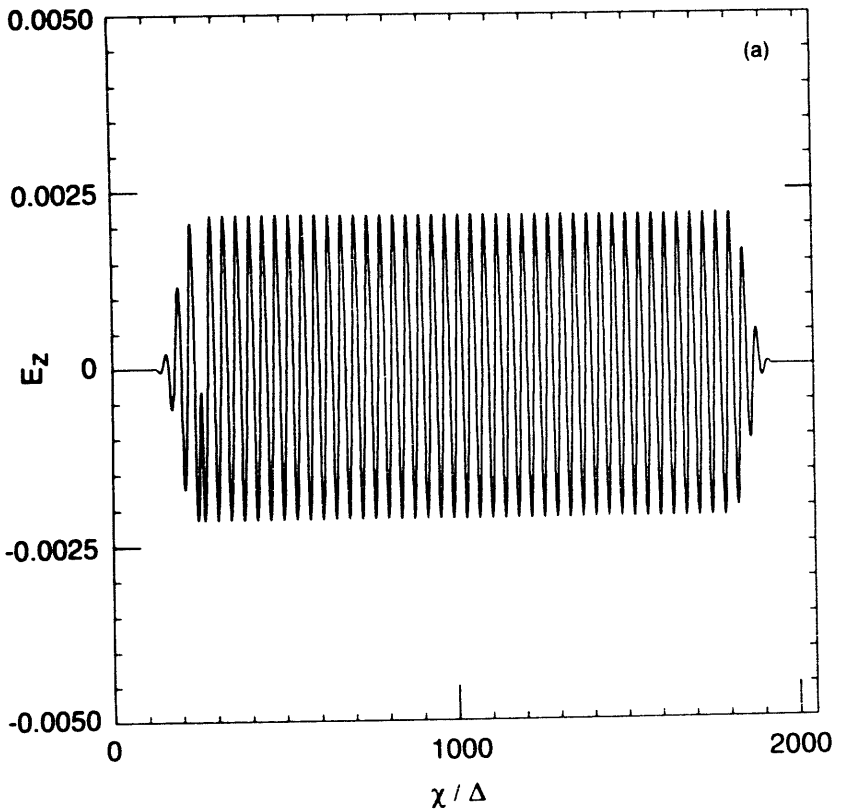
(a)
0.0050
0.0025
0
-0.0025
-0.0050
E_z
0
1000
2000
χ / Δ

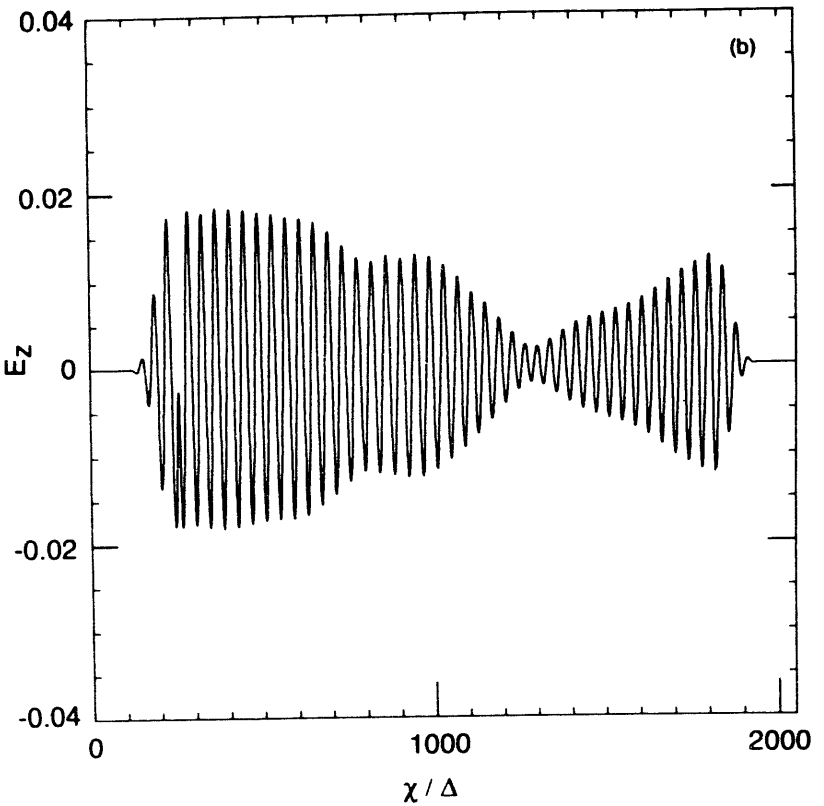
(b)
0.04
0.02
0
-0.02
-0.04
E_z
0
1000
2000
χ / Δ

Fig. 4

PPPL#94X0025

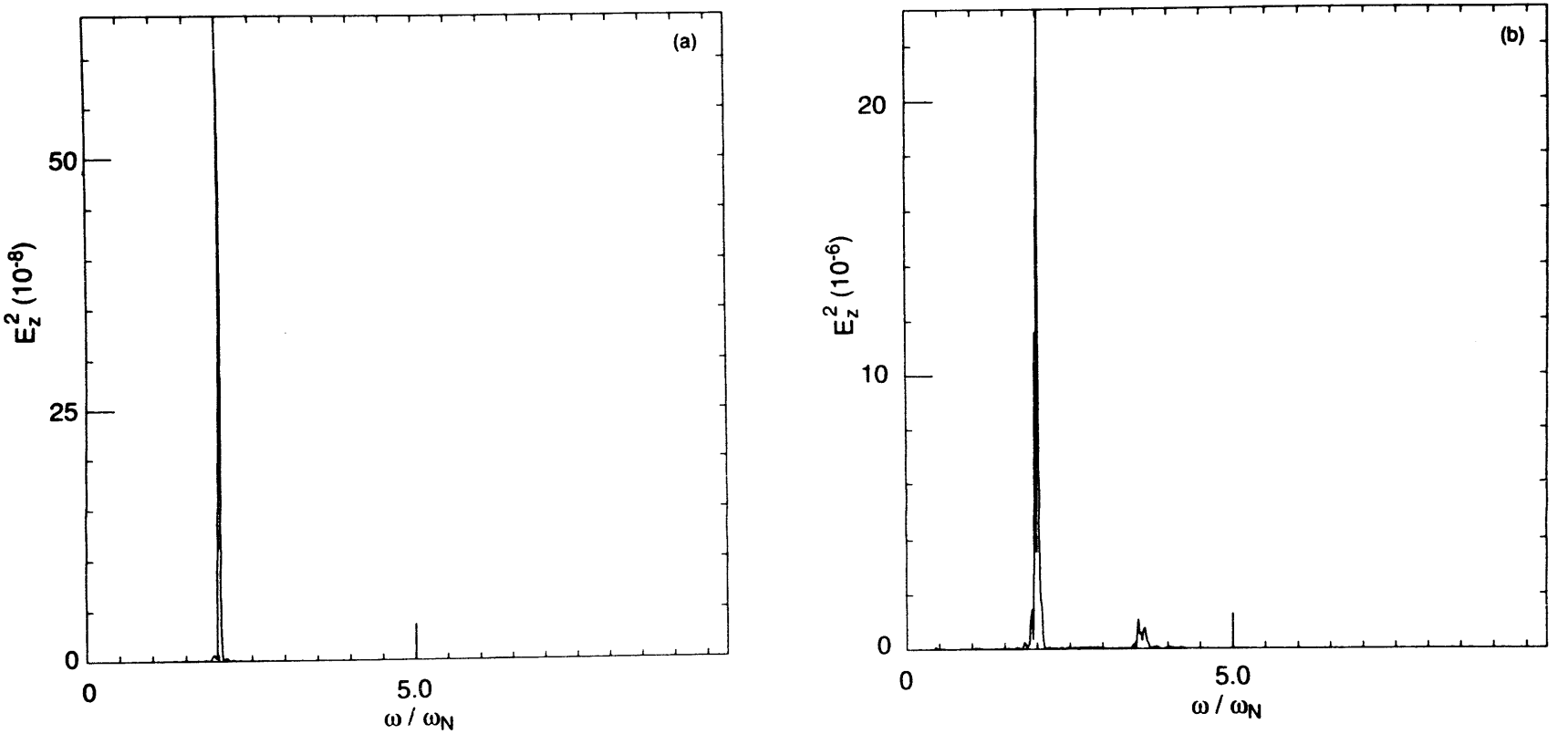
(a)
50
25
0
E_z^2 (10^{-8})
0
5.0
ω / ω_N
(b)
20
10
0
E_z^2 (10^{-6})
0
5.0
ω / ω_N

Fig. 6

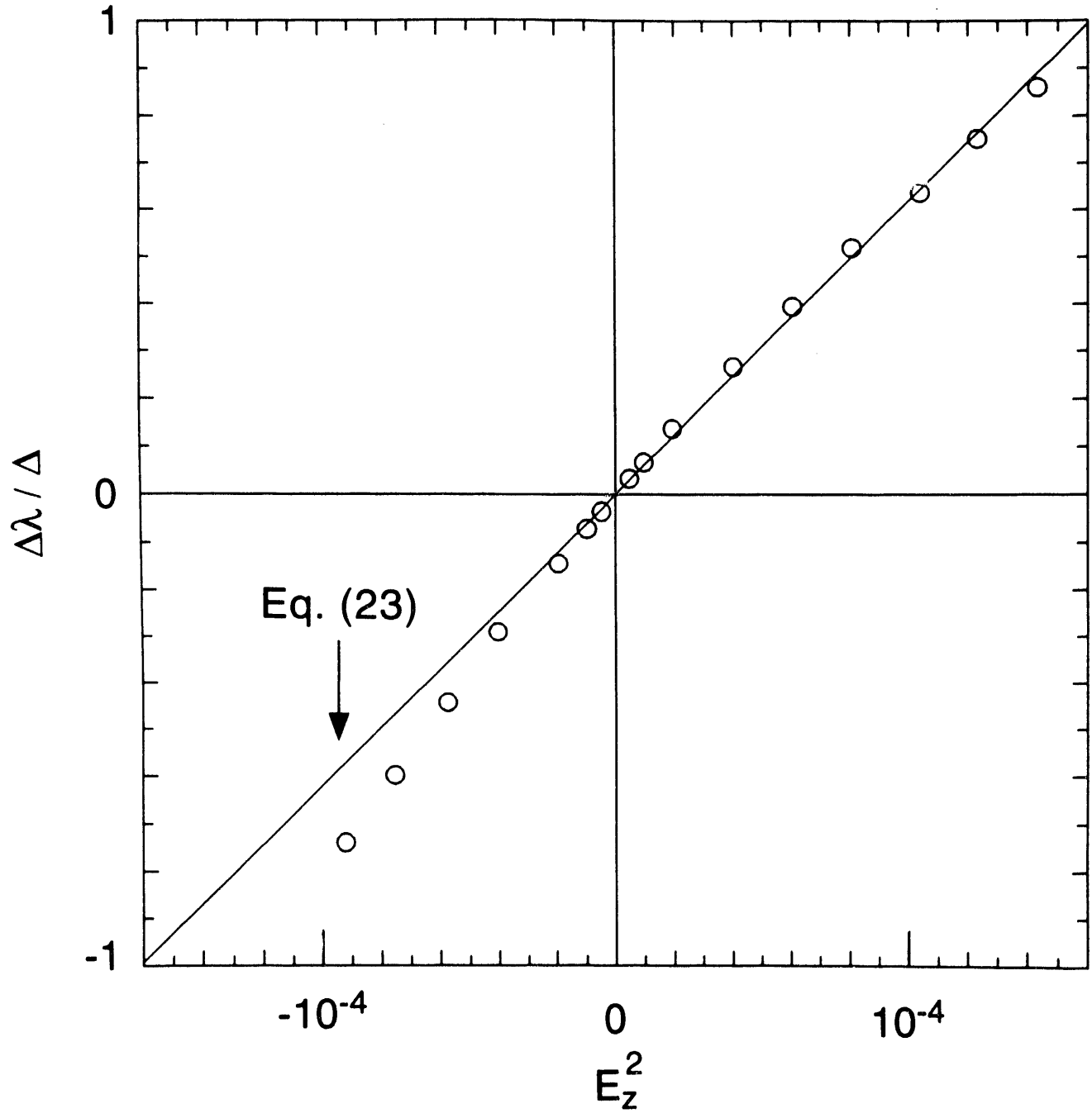

Fig. 7

EXTERNAL DISTRIBUTION IN ADDITION TO UC-420

Dr. F. Paoloni, Univ. of Wollongong, AUSTRALIA
Prof. R.C. Cross, Univ. of Sydney, AUSTRALIA
Plasma Research Lab., Australian Nat. Univ., AUSTRALIA
Prof. I.R. Jones, Flinders Univ, AUSTRALIA
Prof. F. Cap, Inst. for Theoretical Physics, AUSTRIA
Prof. M. Heindler, Institut für Theoretische Physik, AUSTRIA
Prof. M. Goossens, Astronomisch Instituut, BELGIUM
Ecole Royale Militaire, Lab. de Phy. Plasmas, BELGIUM
Commission-European, DG. XII-Fusion Prog., BELGIUM
Prof. R. Boucique, Rijksuniversiteit Gent, BELGIUM
Dr. P.H. Sakanaka, Instituto Fisica, BRAZIL
Prof. Dr. I.C. Nascimento, Instituto Fisica, Sao Paulo, BRAZIL
Instituto Nacional De Pesquisas Espaciais-INPE, BRAZIL
Documents Office, Atomic Energy of Canada Ltd., CANADA
Ms. M. Morin, CCFM/Tokamak de Varennes, CANADA
Dr. M.P. Bachynski, MPB Technologies, Inc., CANADA
Dr. H.M. Skarsgard, Univ. of Saskatchewan, CANADA
Prof. J. Teichmann, Univ. of Montreal, CANADA
Prof. S.R. Sreenivasan, Univ. of Calgary, CANADA
Prof. T.W. Johnston, INRS-Energie, CANADA
Dr. R. Bolton, Centre canadien de fusion magnétique, CANADA
Dr. C.R. James,, Univ. of Alberta, CANADA
Dr. P. Lukác, Komenského Universzita, CZECHO-SLOVAKIA
The Librarian, Culham Laboratory, ENGLAND
Library, R61, Rutherford Appleton Laboratory, ENGLAND
Mrs. S.A. Hutchinson, JET Library, ENGLAND
Dr. S.C. Sharma, Univ. of South Pacific, FIJI ISLANDS
P. Mähönen, Univ. of Helsinki, FINLAND
Prof. M.N. Bussac, Ecole Polytechnique,, FRANCE
C. Mouttet, Lab. de Physique des Milieux Ionisés, FRANCE
J. Radet, CEN/CADARACHE - Bat 506, FRANCE
Prof. E. Economou, Univ. of Crete, GREECE
Ms. C. Rinni, Univ. of Ioannina, GREECE
Preprint Library, Hungarian Academy of Sci., HUNGARY
Dr. B. DasGupta, Saha Inst. of Nuclear Physics, INDIA
Dr. P. Kaw, Inst. for Plasma Research, INDIA
Dr. P. Rosenau, Israel Inst. of Technology, ISRAEL
Librarian, International Center for Theo Physics, ITALY
Miss C. De Palo, Associazione EURATOM-ENEA , ITALY
Dr. G. Grosso, Istituto di Fisica del Plasma, ITALY
Prof. G. Rostangni, Istituto Gas Ionizzati Del Cnr, ITALY
Dr. H. Yamato, Toshiba Res & Devel Center, JAPAN
Prof. I. Kawakami, Hiroshima Univ., JAPAN
Prof. K. Nishikawa, Hiroshima Univ., JAPAN
Librarian, Naka Fusion Research Establishment, JAERI, JAPAN
Director, Japan Atomic Energy Research Inst., JAPAN
Prof. S. Itoh, Kyushu Univ., JAPAN
Research Info. Ctr., National Instit. for Fusion Science, JAPAN
Prof. S. Tanaka, Kyoto Univ., JAPAN
Library, Kyoto Univ., JAPAN
Prof. N. Inoue, Univ. of Tokyo, JAPAN
Secretary, Plasma Section, Electrotechnical Lab., JAPAN
Dr. O. Mitarai, Kumamoto Inst. of Technology, JAPAN
Dr. G.S. Lee, Korea Basic Sci. Ctr., KOREA
J. Hyeon-Sook, Korea Atomic Energy Research Inst., KOREA
D.I. Choi, The Korea Adv. Inst. of Sci. & Tech., KOREA
Prof. B.S. Liley, Univ. of Waikato, NEW ZEALAND
Inst of Physics, Chinese Acad Sci PEOPLE'S REP. OF CHINA
Library, Inst. of Plasma Physics, PEOPLE'S REP. OF CHINA
Tsinghua Univ. Library, PEOPLE'S REPUBLIC OF CHINA
Z. Li, S.W. Inst Physics, PEOPLE'S REPUBLIC OF CHINA
Prof. J.A.C. Cabral, Instituto Superior Tecnico, PORTUGAL
Prof. M.A. Hellberg, Univ. of Natal, S. AFRICA
Prof. D.E. Kim, Pohang Inst. of Sci. & Tech., SO. KOREA
Prof. C.I.E.M.A.T, Fusion Division Library, SPAIN
Dr. L. Stenflo, Univ. of UMEA, SWEDEN
Library, Royal Inst. of Technology, SWEDEN
Prof. H. Wilhelmson, Chalmers Univ. of Tech., SWEDEN
Centre Phys. Des Plasmas, Ecole Polytech, SWITZERLAND
Bibliotheek, Inst. Voor Plasma-Fysica, THE NETHERLANDS
Asst. Prof. Dr. S. Cakir, Middle East Tech. Univ., TURKEY
Dr. V.A. Glukhikh,Sci. Res. Inst. Electrophys.I Apparatus, USSR
Dr. D.D. Ryutov, Siberian Branch of Academy of Sci., USSR
Dr. G.A. Eliseev, I.V. Kurchatov Inst., USSR
Librarian, The Ukr.SSR Academy of Sciences, USSR
Dr. L.M. Kovrizhnykh, Inst. of General Physics, USSR
Kernforschungsanlage GmbH, Zentralbibliothek, W. GERMANY
Bibliothek, Inst. Für Plasmaforschung, W. GERMANY
Prof. K. Schindler, Ruhr-Universität Bochum, W. GERMANY
Dr. F. Wagner, (ASDEX), Max-Planck-Institut, W. GERMANY
Librarian, Max-Planck-Institut, W. GERMANY

DATE
FILMED
8/8/94
END